Communications Earth & Environment https://doi.org/10.1038/s43247-026-03552-6

Article in Press

Hemispheric divergent trends in winter temperature drop days

Received: 6 November 2025

Accepted: 14 April 2026

Cite this article as: Wang, H., Li, J., Zheng, F. *et al.* Hemispheric divergent trends in winter temperature drop days. *Commun Earth Environ* (2026). https://doi.org/10.1038/s43247-026-03552-6

Hao Wang, Jianping Li, Fei Zheng, Matthew Collins & Fei Li

Hemispheric divergent trends in winter temperature drop days

Hao Wang[1,2], Jianping Li[1,3*], Fei Zheng[4,5], Matthew Collins[2*], Fei Li[6]

[1] *Frontiers Science Center for Deep Ocean Multispheres and Earth System-Key Laboratory of Physical Oceanography-Institute for Advanced Ocean Studies-Academy of the Future Ocean, Ocean University of China, Qingdao 266100, China.*
[2] *Department of Mathematics and Statistics, University of Exeter, Exeter, United Kingdom.*
[3] *Laboratory for Ocean Dynamics and Climate, Qingdao Marine Science and Technology Center, Qingdao 266237, China.*
[4] *School of Atmospheric Sciences, Key Laboratory of Tropical Atmosphere-Ocean System, Ministry of Education, Sun Yat-sen University, Zhuhai 519082, China.*
[5] *Southern Marine Science and Engineering Guangdong Laboratory, Zhuhai 519082, China.*
[6] *Jining Meteorological Bureau, Jining 272000, China.*

Submitted to ***Communications Earth & Environment***

* *Corresponding author:*
Prof. Jianping Li
E-mail: ljp@ouc.edu.cn
Prof. Matthew Collins
E-mail: m.collins@exeter.ac.uk

Abstract

As global temperatures rise, widespread warming and fewer cold extremes are generally observed. However, using the metric "temperature drop days", we identify hemispheric divergent trends in winter cold weather over the past four decades. North America experiences increasing temperature drop days, whereas Europe sees a decline, forming a "Cold North America–Warm Europe" pattern. These opposing trends are linked to atmospheric circulation changes: a weakened but asymmetric tropospheric polar vortex has favored more stable circulation over Europe, while a southward-tilting, meandering polar jet enhances daily circulation variability over North America, increasing temperature drop days. Further analysis indicates that this asymmetry primarily arises from tropical Pacific cooling, with contributions from Arctic sea-ice loss, anthropogenic aerosols, and volcanic forcing. In contrast, greenhouse gas forcing mainly drives the overall weakening of the tropospheric polar vortex. Together, this interplay highlights how internal variability and external forcings shape regional winter cold weather.

Key words: Temperature drop day, Climate change, Anthropogenic forcings, Polar vortex, Trend, Cold extremes, Pacific SST

1. Introduction

The recent IPCC Sixth Assessment Report and numerous studies have documented that global warming is driving unprecedented climate changes, including rising air temperatures, increased hot extremes, and reduced cold extremes worldwide[1–7]. While cold extremes still occurred in some regions[8–11], both observational data and climate model projections indicate a continued decline in their frequency and intensity in recent decades and into a warmer future[4,12–16].

Despite these long-term decreasing trends of cold extremes in most areas, significant temperature drops continue to occur from time to time, which sparks the debate on the past trends of cold weather events[9,17,18]. Arctic amplification, which is the enhanced warming in Arctic regions relative to the global average, has been implicated in extreme cold events, particularly in central Eurasia from the 1990s to 2010s[19–24]. It is proposed that Arctic amplification influences mid-to-high latitude weather through the wavier atmospheric circulation, facilitating cold air intrusions from high latitudes[25–27]. However, other studies argue that Arctic amplification weakens mid-latitude cold extremes by reducing meridional temperature gradients[28,29]. Observational evidence consistently shows that, owing to ongoing global warming, air temperatures are rising, and cold extremes are declining in most regions around the world[4,7,30–32].

Existing literature has extensively investigated winter cold extremes, predominantly focusing on cold days defined by absolute low-temperature thresholds or duration[33,34]. Under global warming, there is a broad consensus that the frequency and intensity of such cold extremes are generally decreasing[2,4,15,31,32,34]. However, some studies suggest that cold extremes can persist or even intensify regionally due to atmospheric circulation changes, such as a meandering jet[21,25,26]. While recent global warming has led to a general decline in the frequency of absolute cold extremes, a growing body of literature highlights that cold surges remain a critical component of climate variability[35]. This perspective is crucial as sudden temperature drops pose unique challenges for human health and infrastructure resilience[36,37]. Numerous recent studies have revealed that the overall frequency and intensity of cold surges are generally projected to decrease across the Northern Hemisphere due to anthropogenic warming[38–41], except for certain temporary regional rebounds observed during the recent global warming hiatus[42]. However, a critical gap remains: most prior research has either focused on localized regional changes, particularly over East Asia, or evaluated hemispheric-mean changes. Consequently, the spatial characteristics of long-term trends in temperature drops across the hemisphere, as well as the relative contributions of external forcings and internal climate variability, remain inadequately understood.

Sudden temperature drops have been shown to significantly impact human health, often increasing mortality related to many diseases[43–45]. For instance, exposure to cold can impair respiratory function and trigger the onset or exacerbation of respiratory illnesses[46–48]. Moreover, evidence shows that cardiovascular diseases and mortality, which are believed can be triggered by temperature drop, may increase in temperature drop days[49–52], because exposure to cold without proper protection can raise arterial pressure and lead to increases in coronary and cerebral thrombosis[53]. Notably, numerous studies suggest that cold-related mortality currently far outnumbers the heat-related mortality, underscoring the continued importance of cold weather on public health, even in a warming climate[54–56].

Beyond public health, cold weather events, represented by temperature drop days, also affect socioeconomic systems. Research indicates that fossil fuel consumption increases during cold days, reflecting heightened energy demand[57]. Additionally, large daily temperature fluctuations have been shown to impact retail sector operations[58], investor expectations on asset prices[59], macroeconomic growth, and financial stability[60–63]. Environmental systems are similarly vulnerable to sudden temperature variations. For example, abrupt air temperature changes can damage crop yields[64].

Given these wide-ranging impacts, the question arises: are wintertime cold weather events truly declining in a warming world? In this study, we investigate long-term trends in cold weather by analyzing temperature drop days, defined as days when the daily mean air temperature decreases by more than a specified threshold compared to the previous day (see Methods for details). Winter temperature drop days, often accompanied by strong winds, overcast sky, cold rain and even snowstorms, can disrupt social activities and increase energy consumption. Yet, it remains unclear whether the frequency of temperature drop days has generally declined under recent global warming during the past four decades. To address these questions, we assess the observed trends in temperature drop days over the past four decades using atmospheric reanalysis data. We then explore the potential mechanisms driving these trends, focusing on changes in atmospheric circulation. Finally, we detect the possible effects of tropical Pacific sea surface temperature (SST) trend, sea ice loss and various external anthropogenic and natural forcings on the atmospheric circulation changes.

2. Results

2.1 Observed hemispheric divergent trends in temperature drop days over the past four decades

To evaluate whether trends in the frequency of temperature drop days exhibit similar global uniformity to those of air temperature and cold extremes in the context of recent global warming, we begin by examining the spatial patterns of trends in winter temperature drop day frequency using reanalysis datasets. Fig. 1a illustrates the observed linear trends in the frequency of winter temperature drop days over the past four decades. Surprisingly, in contrast to the trends observed in air temperature and cold extremes, the frequency of temperature drop days displays significant spatial heterogeneity. In the Northern Hemisphere, despite rising air temperatures and a decline in cold extremes, the frequency of temperature drop days does not exhibit a uniform decrease. In many regions, the frequency remains stable or even increases substantially in the context of ongoing global warming. Notably, in terrestrial regions, winter temperature drop days have become more frequent in central and western North America, parts of South Asia, and certain regions of China, suggesting that residents in these areas are experiencing more days with noticeable temperature drops during winter. In contrast, large portions of northern and western Europe have experienced a decline in winter temperature drop days, indicating fewer cold spells. Isolated regions in tropical Africa and Russia also show a decreasing trend. Additionally, the frequency of temperature drop days has increased across several oceanic regions. These findings are based on a threshold of 1.0 standard deviation to identify temperature drop days, with additional analysis conducted using thresholds of 1.5 and 2.0 standard deviations to assess the spatial distribution of trends in winter temperature drop day frequency (Supplementary Fig. 1). The spatial patterns across these thresholds are generally consistent, suggesting that the results are robust to variations in the threshold selection.

To assess the relative magnitude of these trends, it is essential to consider the climatological mean. The spatial distribution of the mean winter temperature drop day frequency is shown in Supplementary Figure 2. On average, these cold events occur approximately 12.7 days per winter across the Northern Hemisphere (defined by the 1.0 STD threshold). This indicates that these events typically occur on about 14% of winter days. For example, in North America, the observed linear trend is approximately +0.5 to +1.0 days/decade (Fig. 1a). Over the past four decades, this accumulates to an increase of roughly 2.5 to 4.5 days. Compared to the climatology of ~12 days, this represents a substantial relative increase of 20%–40%.

A striking feature of these spatially disparate trends is the observed contrasting trends in two major regions: central and western North America and northern and western Europe. These contrasting trends suggest the emergence of a "Cold North America–Warm Europe" (CNWE) pattern, which highlights a hemispheric divergence of temperature drop day trends. To quantify this large-scale hemispheric divergence in temperature drop day frequency trends, we constructed a CNWE index based on the annual frequency of winter temperature drop days in these two regions with opposing trends (Fig. 2a; also see Methods for details). This index is calculated as the difference between the standardized temperature drop day frequency anomalies over North America (30°–40°N, 100°–115°W) and Northern Europe (55°–65°N, 30°–50°W). The Empirical Orthogonal Function (EOF) leading mode captures the dominant mode of interannual variability of winter temperature drop day frequency (Fig. 2b). While the center of the EOF pattern is located over central North America, it exhibits a coherent sign across nearly the entire continent, indicating that the interannual variability of winter temperature drop day frequency tends to be similar across the region. Although the maximum center of the linear trend is slightly displaced to the west compared to the EOF center, both analyses highlight the same broad region of variability. Fundamentally, the linear trend projects onto this dominant EOF mode in North America (Fig. 2b). Temporal variations in the CNWE index closely align with those of the first principal component (PC) time series, with a correlation coefficient exceeding 0.85 (Fig. 2c). The spatial pattern of the first principal component closely mirrors the trend patterns in temperature drop day frequency (Fig. 2b), suggesting that the CNWE index effectively reflects the temporal evolution of global spatial disparities in winter temperature drop day frequency. We further verified that the trends in both individual regions of the index, the increasing frequency in North America and the decreasing frequency in Europe, are both statistically significant, ensuring that the CNWE index reflects a robust hemispheric divergence rather than a signal solely dominated by a single region. Notably, the CNWE index exhibits a significant upward trend (Fig. 2a), indicating a global shift in the frequency of temperature drop days toward the CNWE pattern, characterized by the hemispheric divergent trends in winter temperature drop days.

To further confirm this spatial disparity, we compare the CNWE index between the pre- and post-2000 periods. Fig. 1b presents the probability distribution of bootstrapped CNWE index anomalies for both periods, revealing that the index is significantly higher in the past two decades compared to the pre-2000 period. This indicates that winter temperature drop days have become more frequent in North America, while their frequency has declined in Europe, reinforcing the notion of hemispheric heterogeneous trends under global warming over the last four decades.

Building on this, we assess the spatial extent of divergent trends in winter temperature drop day frequency by comparing the area coverage of different trend types (Fig. 1c). Despite significant global increases in air temperature and reductions in cold extremes, temperature drop days have not shown widespread decreases in most regions. In the Northern Hemisphere, substantial areas show no significant trend, and the spatial extents of regions with significant increases (2.12×10^7 km^2) and decreases (2.25×10^7 km^2) in winter temperature drop day frequency have been broadly comparable even though there is widespread warming over the past four decades. This spatial pattern stands in stark contrast to the winter near-surface air temperature trends (Fig. 1d), which show a nearly universal significant warming across most regions, with very few areas exhibiting any cooling trends. These findings further emphasize the spatially disparate trends in winter temperature drop day frequency.

2.2 The role of atmospheric circulation changes in the hemispheric divergent trends

The trends in temperature drop days are likely driven by changes in atmospheric circulation, as atmospheric circulation is a key determinant of air temperature variability. Fig. 3 illustrates the observed trends in winter atmospheric circulation over the past four decades, revealing an overall increase in geopotential heights across much of the Northern Hemisphere and a general weakening of the tropospheric polar vortex (TPV) as previous studies suggested[6,65–67]. However, this reduction in the TPV intensity is uneven and zonally asymmetric, with the most pronounced decline over Northern Europe, while much weaker and insignificant decline over the side of North America (Fig. 3c, d)[68]. This suggests that the TPV may be more frequently displaced toward North America, potentially leading to increased daily atmospheric circulation variability there. Consequently, the TPV appears to have a more pronounced impact on the atmospheric circulation over North America, while the atmospheric circulation over Europe remains relatively stable.

Winter temperature drop days are closely linked to daily changes in atmospheric circulation, with several studies highlighting the significant influence of atmospheric thickness variability on air temperature[69–71]. Analyzing daily changes in atmospheric circulation, a reduction in atmospheric thickness is associated with a temperature drop. To further explore the relationship between the hemispheric divergent trends, represented by the CNWE pattern, and changes in atmospheric thickness, we examine the frequency of atmospheric thickness drop days (Supplementary Fig. 3). The CNWE index exhibits a significant positive correlation with 500–1000 hPa atmospheric thickness drop day frequency over North America, and a significant negative correlation over Europe. This indicates that an increasing frequency of atmospheric thickness drop days over North America, with a decreasing frequency over Europe, may contribute to the spatial disparities in temperature drop days, as characterized by the CNWE pattern. Additionally, we observe a Pacific-North American (PNA) teleconnection-like pattern in the atmospheric circulation associated with the CNWE index. Over the past four decades, a long-term cooling trend in tropical eastern Pacific SST has been observed[72], which may exert a sustained influence on atmospheric circulation over North America and potentially contribute to the formation of the CNWE pattern via teleconnection.

To verify the dynamical features of atmospheric circulation on temperature drop days, we performed a composite analysis of atmospheric circulation anomalies on temperature drop days. As shown in Supplementary Fig. 4, the temperature drop days in most areas of North America are coincident with significant cold air advection which could be driven by the northwest-to-southeast tilting of the polar jet stream. It is clear the cold advection in the western North America is milder than in the central North America. This spatial offset is possibly attributed to topographical effects. The complex and mountainous topography in western North America acts as barriers, disrupting the low-level wind fields and weakening the horizontal cold advection. In contrast, the central and eastern parts of North America are characterized by flat plains. The lack of topographic blocking allows the cold, dense air to surge rapidly southeastward. This unobstructed flow sustains much stronger cross-isotherm winds and sharper temperature gradients. Consequently, the absolute maximum of the cold advection term anchors over the central and eastern region. For the temperature drop days in Europe, it is also clear that there is significant anomalous cold advection in central and eastern Europe, which drives the temperature drop days. Then, Supplementary Fig. 5 shows the composite 500–1000 hPa atmospheric thickness anomalies on winter temperature drop days for North America and Northern Europe, respectively. Whether for North America or Northern Europe, the 500–1000 hPa atmospheric thickness fields exhibit significant negative anomalies on the temperature drop days. This implies that the atmospheric thickness becomes anomalously shallow on temperature drop days. According to the perturbation hypsometric equation, this dynamically driven thickness reduction forces the air column to cool rapidly to reach a new hydrostatic balance[69,73]. Therefore, there will be a temperature drop when the atmospheric thickness becomes anomalously thin. The above results indicate that both the horizontal temperature advection and atmospheric thickness reduction could drive the temperature drop days.

Then, to connect the above dynamical feature to the polar vortex, we further analyzed the 200 hPa zonal wind anomalies for the temperature drop days in North America, as the zonal wind anomaly directly represents the westerly jet stream change. Supplementary Fig. 6 reveals two distinct, opposing dipole patterns. Over the Northeast Pacific, there is a "positive-North, negative-South" anomaly dipole, which strengthens westerlies to the north but weakens to the south, indicating a poleward displacement of the jet stream. Conversely, over North America, a reversed "negative-North, positive-South" dipole appears, indicating an equatorward shift of the jet stream, which signifies a southward excursion of the TPV. These opposing dipoles with a deep troughing structure over the western North America facilitate the southward intrusion of cold air from the north (Supplementary Fig. 4a), and favors the reduction in atmospheric thickness (Supplementary Fig. 5a).

Given the long-term trends in the TPV and the role of daily atmospheric circulation changes in driving spatial disparities in temperature drop day frequency, we next examine long-term trends in daily atmospheric circulation variability. Fig. 4 displays trends in wintertime daily atmospheric circulation variability from 1979 to 2024, including the frequency of the westerly jet and the frequency of 500–1000 hPa atmospheric thickness drop days. The polar jet, located around mid- to high latitudes, is a primary driver of weather patterns in the mid- to high latitudes, sees a shift in its occurrence position across the Northern Hemisphere (Fig. 4a). A dipole trend pattern is observed in polar jet frequency over the North Pacific, with a positive trend in the north of the jet axis and a negative trend to the south. This suggests a poleward displacement of the polar jet over the North Pacific over the past four decades[6]. In contrast, over North America, the dipole pattern reverses, with a positive trend in westerly jet frequency to the south of the jet axis and a negative trend to the north. This indicates the tendency of a southward shift of the polar jet relative to its climatological location over North America. Therefore, by overlaying the trends on the climatological position, we can clearly see the displacement of jet stream with the deepening of the North American trough, which facilitates the southward intrusion of cold air to North America. These shifts combine to produce a more meandering jet stream, consistent with previous studies[25,26,74]. This meandering polar jet stream tilts from northwest to southeast across central and western North America, promotes more frequent northerly flows and increased daily atmospheric circulation variability, as indicated by the heightened frequency of 500–1000 hPa atmospheric thickness drop days over North America (Fig. 4b). As a result, temperature drop days occur more frequently in this region. Conversely, due to the aforementioned more stable atmospheric circulation over Northern Europe, driven by the weaker TPV in this region (Fig. 3), the frequency of daily 500–1000 hPa atmospheric thickness drop days has decreased over Northern Europe. Consequently, winter temperature drop days have become less frequent. Thus, the hemispheric contrasting trends in daily atmospheric circulation variability have led to opposite trends in temperature drop day frequencies over North America and Europe, reinforcing the hemispheric divergence characterized by the CNWE pattern.

In addition to these trends in atmospheric thickness, variability in daily wind changes further reflects the divergent atmospheric circulation trends. Supplementary Fig. 7 presents observed trends in the variability of daily wind changes over the past four decades. For both zonal (Supplementary Fig. 7a) and meridional (Supplementary Fig. 7b) winds, the variability of daily wind changes has increased over North America, while it has decreased over Northern Europe. This indicates more frequent variations in wind intensity and direction over North America, whereas such variations have become less common over Northern Europe. These changes in daily wind variability could further contribute to the observed differences in daily air temperature fluctuations over the two regions.

These findings indicate that daily atmospheric circulation variability has increased over North America while decreasing over Northern Europe over the past four decades. As a result of these hemispheric contrasting circulation changes, temperature drop days have become more frequent in North America while less frequent in Northern Europe, leading to the CNWE pattern which is characterized by opposing trends in these regions, and highlighting the hemispheric divergent trends in winter temperature drop days.

2.3 Influence of external forcings and SST trends on atmospheric circulation

The results above highlight that atmospheric circulation changes are central to the emergence of the CNWE pattern, with daily variability linked to an asymmetric weakening of the TPV between North America and Northern Europe. A key question, therefore, is what drives this hemispheric asymmetry. To address this, we analyze simulations from both Atmospheric Model Intercomparison Project (AMIP) and fully coupled historical runs, as well as targeted forcing experiments from the Detection and Attribution Model Intercomparison Project (DAMIP) within Coupled Model Intercomparison Project Phase 6 (CMIP6)[75,76].

Previous studies have shown that CMIP6 historical simulations generally reproduce a global warming pattern. However, over the past four decades, the tropical Pacific has exhibited a cooling trend that is at odds with these simulations[72]. To isolate the potential influence of this long-term cooling in the tropical eastern Pacific, we compare AMIP simulations, which are forced with observed SST and sea ice, with fully coupled historical simulations.

We begin by comparing the prescribed observed SST and sea ice trends with those simulated in historical runs to determine the primary drivers of the AMIP-Historical discrepancy (Supplementary Figs. 8 and 9). For SST, as shown in Supplementary Fig. 8, there is a striking contrast in the tropical Pacific. The observation exhibits a clear long-term cooling trend in the tropical eastern Pacific (Supplementary Fig. 8a). However, the historical simulation shows a broad warming trend across the entire tropical Pacific, failing to capture the tropical eastern Pacific cooling (Supplementary Fig. 8b). The difference map (Supplementary Fig. 8c) highlights a significant warm bias in the historical runs over the tropical eastern Pacific. This discrepancy aligns with the “SST pattern effect”, which shows that current coupled climate models have systematic biases in simulating the observed pattern of SST change, especially in tropical eastern Pacific[72,77]. This confirms that using the difference between AMIP and historical simulations could represent the effect of the long-term cooling trend in tropical eastern Pacific. We also assessed the boreal winter sea ice trends in Supplementary Figure 9. It is clear that the historical simulation generally reproduces the decline of Arctic sea ice (Supplementary Fig. 9b). However, discrepancies appear in the Barents-Kara Seas (BKS) and Chukchi–Bering Seas (CBS). Observations show a massive sea ice loss in the BKS region (Supplementary Fig. 9a), whereas the historical multi-model ensemble (MME) mean simulates a weaker decline than the observation (Supplementary Fig. 9b). However, for the CBS region, the models overestimate the sea ice loss. Although the contrast of sea ice between the observation and historical simulation is not as sharp as SST, the difference between AMIP and historical simulations may also involve some effect from the declining BKS and CBS sea ice. The Arctic sea ice loss may be a potential factor for the CNWE pattern but without separate SST and sea-ice forced experiments it is difficult to quantify the relative roles of the two factors. This could be an interesting avenue for future research.

Differences between these two types of simulations can, to some extent, primarily capture the contribution of the tropical eastern Pacific cooling trend, plus some effect from Arctic sea ice loss, although they may also involve some effect from the SST trends in other regions (such as the Southern Ocean). Before comparing the linear trends of AMIP and historical simulations, we briefly evaluate if the model could capture the climatology of winter temperature drop day frequency. As shown in Supplementary Fig. 10, both AMIP and CMIP6 historical simulations generally reproduce the observed climatological frequency of temperature drop days. The spatial patterns for observations, AMIP and CMIP6 historical runs are similar. This indicates that the models could capture the basic features of the climatology of temperature drop day frequency in winter. As shown in Fig. 5a, the winter temperature drop day frequency exhibits pronounced discrepancies between AMIP and CMIP historical simulations over North America: AMIP simulations produce a substantially stronger positive trend than CMIP historical simulations. This suggests that the tropical Pacific cooling trend may contribute to the observed increase in winter temperature drop days in North America. In contrast, there are differences between observations (Fig. 1a) and model difference (Fig. 5a) around high-latitude Asia (around 40°–60°N, 60°–140°E). This implies that the Pacific SST cooling tends to induce opposite signals in high-latitude Asia, and the mismatch between observations and model difference confirms that the long-term increasing trends in temperature drop days over Asia (parts of central Asia, south-central Siberia, and southwestern to central-western China) are not primarily driven by Pacific SST, but rather by other factors. Nevertheless, it is important to note that observed SST trends differ from historical simulations in other ocean basins as well, and the BKS sea ice declining trend is underestimated while the CBS sea ice declining is overestimated in historical simulations (Supplementary Fig. 9c). These discrepancies could also influence the results.

To more directly assess the role of the tropical Pacific SST trend in shaping the CNWE pattern, we compare CNWE indices between AMIP and historical simulations (Fig. 5b). In terms of the CNWE index trend, the historical MME mean exhibits a positive trend, consistent with the sign of the observed trend. However, the magnitude of the trend in historical simulations is weaker than in AMIP and observations. This confirms that the lack of this SST driver, and the competing effects from different external forcings, significantly dampens the signal in coupled historical runs. Both the MME and 10 out of 12 individual models show markedly larger positive trends in the CNWE index in AMIP than in historical simulations. These consistent results indicate that the long-term cooling of the tropical eastern Pacific SST may exert a potential influence on the CNWE pattern, with the effect from Arctic sea ice loss, particularly by enhancing the occurrence of winter temperature drop days over North America.

To evaluate the influence of external forcings on asymmetric patterns, Fig. 6 shows the zonally asymmetric components of trends in large-scale winter atmospheric circulation under different forcing scenarios. Under greenhouse gas (GHG) forcing, the TPV exhibits an overall weakening (Supplementary Fig. 11a, d), promoting a more stable large-scale circulation. However, this decline does not exhibit the asymmetric pattern facilitating the CNWE pattern. Notably, the decrease in the TPV intensity is somewhat more pronounced over North America than over Northern Europe (Fig. 6a, d). Although the overall reduction in the TPV intensity is absent under both anthropogenic aerosol (AER) and natural (NAT) forcings, the effects of these two factors on the shift of the TPV are asymmetric. In the case of AER forcing, the intensity of the TPV weakens over Europe, while it remains nearly unchanged over North America (Supplementary Fig. 11b, e). This finding suggests that AER forcing may exert asymmetric effects on the TPV intensity, especially on the weakening over Northern Europe (Fig. 6b, e). Similarly, under NAT forcing, the TPV exhibits distinct asymmetric changes in intensity. Specifically, the intensity of the TPV increases under natural forcing, with a notable intensification over North America (Supplementary Fig. 11c, f). This result indicates that natural forcing also facilitates the asymmetric TPV shift (Fig. 6c, f).

Consistent with the spatial patterns, the largest hemispheric asymmetries in the TPV trends occur under AER forcing, followed by NAT forcing (Fig. 6g, h), indicating that both forcings make substantial contributions to the longitudinal heterogeneity of vortex changes. In contrast, GHG forcing produces a weak response of opposite sign, suggesting a minimal influence on the asymmetric component of the TPV weakening. Notably, the AMIP simulations also exhibit pronounced hemispheric asymmetry, which is greater than that in any individual external forcing experiment, highlighting the potential importance of the long-term cooling trend in tropical Pacific SST in driving this asymmetry in atmospheric circulation. Taken together, these results point to a possible dominant role of tropical Pacific SST cooling, supplemented by contributions from the regional Arctic sea ice loss, external AER and NAT forcings, in shaping the zonally asymmetric signal.

To further explore the influence of natural forcings on zonally asymmetric shift in the TPV, we compared the zonally asymmetric components of geopotential height changes under different NAT forcing scenarios (Supplementary Fig. 12). The patterns associated with volcanic (VOLC) forcing closely mirror those under NAT forcing (Supplementary Fig. 12a, c), whereas solar (SOL) forcing exhibits somewhat differences from NAT forcing (Supplementary Fig. 12b, d). Notably, the time series reveal a stronger positive trend in geopotential height differences under VOLC forcing, suggesting a stronger decline in the TPV intensity over northern Europe compared to North America (Supplementary Fig. 13). These results suggest that VOLC forcing may be a key driver of the zonally asymmetric shift of the TPV among NAT forcings.

By isolating the contributions of different forcing factors, it becomes apparent that the overall decline in the TPV intensity is primarily driven by GHG emission, while the hemispheric uneven changes in intensity are mostly attributable to the tropical eastern Pacific SST trend, with additional effect from the regional Arctic sea ice loss, aided by AER and NAT forcings. And VOLC forcing may play an important role among NAT forcings. This result reveals that the combined influence of SST trend, anthropogenic and volcanic forcings jointly contributes to the long-term changes in the TPV, thereby shaping the CNWE pattern.

3. Discussion

Previous observational studies have shown that global warming has led to general increases in air temperature and decreases in cold extremes across most regions worldwide. However, the present study reveals spatially disparate trends in the frequency of winter cold weather, represented by temperature drop days, over the past four decades. Notably, the spatial extents of regions with significant increases and decreases in the frequency of winter temperature drop days are similar, suggesting that climate change could lead to more frequent winter temperature drop days in certain regions. Specifically, North America has experienced an increase in the frequency of temperature drop days, while northern Europe has seen a decline, thereby giving rise to hemispheric divergent trends featured with the CNWE pattern.

This phenomenon is closely tied to changes in atmospheric circulation. Overall, there has been a general decline in the intensity of the TPV, with the most pronounced weakening occurring over Europe, which has resulted in more stable atmospheric circulation in that region. However, the decrease in the TPV intensity is asymmetric, with a much weaker and statistically insignificant decrease over North America. Consequently, the TPV appears to exert a stronger influence on daily atmospheric circulation in North America. The trends in daily polar jet frequency display opposing north-south dipole patterns, indicating a poleward shift over the North Pacific, while an equatorward shift over North America. This meandering jet stream, which tilts from northwest to southeast across central and western North America, enhances daily atmospheric circulation variability. This variability is reflected in more frequent changes in wind direction and intensity, as well as increased frequency of atmospheric thickness drop days, both of which contribute to more frequent temperature drop days in North America. Conversely, the more stable atmospheric conditions over northern Europe, driven by the weaker TPV, result in a decrease in the frequency of thinned atmospheric layers and, consequently, fewer temperature drop days. These contrasting trends in atmospheric circulation variability explain the hemispheric divergent trends in temperature drop day frequency characterized with the CNWE pattern.

Further analysis using model outputs from the AMIP, historical and DAMIP within CMIP6 indicates that GHG forcing plays a primary role in the overall weakening of the TPV, which leads to a more stable atmospheric circulation. However, the long-term SST trend (possibly the cooling trend in tropical eastern Pacific), appear to dominate the asymmetric and hemispheric uneven changes in the TPV intensity, with some additional effects from the reginal Arctic sea ice loss, external AER and NAT forcings. These results suggest that the observed large-scale atmospheric circulation changes, which give rise to the CNWE pattern, could be primarily attributed to SST trends, with additional effects from the regional Arctic sea ice loss, external anthropogenic and NAT forcings, and volcanic forcing plays a more important role among NAT forcings.

Are most temperature drop days above normal daily mean air temperatures? We quantitatively examined whether the identified “temperature drop days” correspond to anomalously cold days. We calculated the percentage of temperature drop days (defined by 1.0 STD threshold) where the daily mean temperature is lower than the local climatological mean temperature for that day. As shown in Supplementary Figure 14, in the vast majority of the Northern Hemisphere, particularly over land areas like North America and Eurasia, most of the temperature drop days exhibit daily air temperatures below the climatology. For North America (Europe), the proportion is 75.96% (79.98%). This confirms that while our definition focuses on the “temperature drops”, most days are anomalously cold days. Cases where an “extremely warm day is followed by a slightly warm day” represent a small minority of temperature drop days.

It should be noted that we focus on the trends in winter temperature drop day in the Northern Hemisphere, while further assessment is needed for the Southern Hemisphere, where different influencing factors may exist. Additionally, while our study mainly focuses on the CNWE pattern, we note that East Asia also exhibits increasing trends in winter temperature drop days over some areas (Fig. 1a). However, the tropical Pacific SST cooling primarily drives the increasing trends in North America, and it may have opposite effect on Asia. The mismatch between observations and model difference in Asia implies that the temperature drop day trends are not primarily driven by Pacific SST, but rather by other factors, warranting more detailed analysis.

Furthermore, while this study attributes the hemispheric divergent trends in winter temperature drop days, particularly the opposing trends in North America and Europe, to long-term atmospheric circulation changes in a warming climate, the detailed effects of other internal factors should also be considered. Regarding the role of the cryosphere, observational analysis reveals that the CNWE pattern is significantly correlated with sea ice variability in the BKS and Eurasian snow cover (Supplementary Fig. 15), indicating that Eurasian snow cover decline and BKS sea ice loss are closely linked to the CNWE pattern. Although CMIP6 historical simulations could capture the BKS sea ice loss, this regional sea ice loss tends to be underestimated (Supplementary Fig. 9). This regional bias likely explains why CMIP historical simulations produce a weaker CNWE signal compared to observations. It is also worth noting that the CMIP6 historical simulations overestimate the CBS sea ice loss, and the CBS sea ice is negatively correlated with CNWE index. Therefore, we conclude that the CNWE pattern is primarily shaped by the tropical Pacific SST cooling, with the additional effect of the Arctic sea ice loss. Thus, the Arctic sea ice, a critical driver of polar atmospheric circulations, has been shown to influence cold weather patterns in the mid-high latitudes[29,78], pointing to a need for further investigation into the role of sea ice changes. A long-term cooling trend in tropical eastern Pacific SST is also identified[72]. Tropical SSTs, particularly over the Pacific, play a crucial role in linking tropical climate change to mid- and high-latitude weather and climate through atmospheric teleconnections[79]. In this study, by combining AMIP and historical simulations, we propose that tropical Pacific SSTs may serve as a potential dominant driver of anomalous atmospheric circulation changes over North America via a PNA-like teleconnection pattern. This large-scale teleconnection directly modulates the atmospheric circulation anomalies over the North Pacific and western North America, thereby altering the position and meandering of the polar jet stream, which subsequently modulate the local synoptic atmospheric circulation over North American and shapes the CNWE pattern. However, further detailed analysis is needed to fully understand this relationship.

Methods

Reanalysis and observational data

The fifth generation European Centre for Medium-Range Weather Forecasts (ECMWF) atmospheric reanalysis dataset (ERA5) is employed[80]. The ERA5 has a horizontal resolution of 0.25° × 0.25°, and is available from 1940 to present. The daily atmospheric variables, including 2m air temperature, geopotential, U- and V-component of winds, and monthly sea ice cover and snow cover are used in the study.

To examine the difference in sea surface temperature (SST) trends between observational and model data, we utilized the monthly mean SST data from the Hadley Centre Global Sea Ice and Sea Surface Temperature (HadISST) dataset, version 1.1[81]. This dataset is provided on a global 1° × 1° grid from 1870 to present.

This study focuses on the period from 1979 to 2024. This period coincides with the beginning of the satellite era, ensuring high quality for daily data, and to focus on the era of rapid global warming.

CMIP6 model data

Daily near surface air temperature, monthly geopotential height, sea surface temperature and sea ice area percentage in model outputs from the Detection and Attribution Model Intercomparison Project (DAMIP), historical and AMIP simulations within CMIP6 are employed (see Supplementary Table 1 for details)[75,76]. To investigate trends in large-scale atmospheric circulation, and its relationship with CNWE index, simulations of historical greenhouse gas (hist-GHG), anthropogenic aerosol (hist-aer), natural (hist-nat), solar (hist-sol) and volcanic (hist-volc) forcings spanning 1979 to 2020 are analyzed. We also use AMIP and historical simulations to explore the potential influence from SST and sea ice trends on the CNWE pattern, and the time span available for AMIP and historical simulations is up to December 2014.

Temperature drop day frequency

In this study, we focus on the boreal winter season, defined as the period from December 1st to February 28th. For instance, the winter of 2000 spans from December 1st, 2000, to February 28th, 2021.

The temperature drop day is defined based on the daily temperature difference. The daily temperature change (ΔT) is calculated as the difference in daily mean air temperature between a given day (t) and the preceding day ($t-1$):

$$\Delta T_t = T_t - T_{t-1} \quad (1)$$

where ΔT_t is the daily temperature difference on the given day t. T_t and T_{t-1} are the daily mean air temperature on the given day t and the preceding day, respectively.

A temperature drop day is identified as a day with a temperature drop exceeding a specific threshold compared with the preceding day. Specifically, if the daily temperature difference on a given day (ΔT_t) falls below −1.0 standard deviation (σ) of the daily temperature differences across all winters, that day is classified as a temperature drop day:

$$\Delta T_t \leq -1.0 \times \sigma \quad (2)$$

where σ is calculated using daily temperature difference for all winter days over the climatological baseline period (1979–2024). This relative threshold ensures that the metric captures temperature drop days pertinent to each region's specific variability.

Finally, the winter temperature drop day frequency is defined as the total count of identified temperature drop days within each winter season.

Cold North America–Warm Europe (CNWE) index

To quantify the hemispheric divergent trends in winter temperature drop day frequency, we defined the Cold North America–Warm Europe (CNWE) index. This index captures the two key regions with opposite trends identified in the trend analysis (Fig. 1a).

The CNWE index is defined as the difference between the standardized area-averaged winter temperature drop day frequency in North America (30°–40°N, 100°–115°W), and that in Europe (55°–65°N, 30°–50°E).

The CNWE index has a significant increasing trend, and its positive phase signifies a "Cold North America–Warm Europe" pattern, characterized by more frequent temperature drop days in North America and fewer in Europe.

Atmospheric thickness drop day frequency

Air temperature change is influenced by atmospheric thickness change. According to previous studies, positive atmospheric thickness anomaly corresponds to the rise in air temperature, while the atmospheric thickness reduction induces air temperature drop based on the perturbation hypsometric equation[69,73]. In this study, 500–1000 hPa atmospheric thickness is analyzed.

Assuming dZ_t is the daily mean atmospheric thickness on the day t, the daily atmospheric thickness change can be expressed as:

$$\Delta dZ_t = dZ_t - dZ_{t-1} \quad (3)$$

where ΔdZ_t is the daily atmospheric thickness change on the day t. dZ_{t-1} is the daily mean atmospheric thickness on the day $t-1$.

Therefore, similar to the definition of temperature drop day frequency, we define the atmospheric thickness drop day frequency to explore the possible influence of regional daily atmospheric circulation change on temperature drop days based on −1.0 standard deviation of the daily atmospheric thickness change for all winters. If the atmospheric thickness on a given day drops compared to the previous day, and the magnitude of the drop exceeds 1.0 standard deviation of all the daily atmospheric thickness change, then this day can be defined as an atmospheric thickness drop day.

Westerly jet frequency

To characterize the daily circulation variability and spatial shifts of the polar jet stream, we utilized the westerly jet frequency based on the 200 hPa zonal wind.

A "westerly jet day" is identified at a specific grid point if the daily zonal wind speed exceeds 30 m s^{-1}. The westerly jet frequency is then calculated as the total count of such days within each winter season.

The trends in westerly jet frequency effectively capture the spatial displacement and meandering of the jet stream. For instance, an increasing trend in jet frequency at lower latitudes with a decreasing trend at higher latitudes signifies a systematic southward displacement.

Statistical methods

The trends reported in this study are calculated using the Theil-Sen trend estimation method, which, unlike simple linear regression, is robust to outliers and provides more reliable trend estimates[82].

The Mann-Kendall (M-K) test, which is a non-parametric trend significance test, is used to assess the significance of trends in time series[83,84].

The bootstrap method, a data resampling technique particularly useful for small sample sizes[85], is employed to determine shifts in mean CNWE index anomalies between two past periods. For this analysis, 10,000 bootstrapped composites are generated based on the CNWE index anomalies for the two periods.

Data availability

The ERA5 atmospheric reanalysis data is accessible at https://cds.climate.copernicus.eu/datasets/reanalysis-era5-complete?tab=overview. The HadISST can be accessed from https://www.metoffice.gov.uk/hadobs/hadisst/index.html. The CMIP6 model data is available through https://esgf-node.llnl.gov/projects/cmip6/.

Code availability

The NCAR Command Language (NCL) and Python are used to visualize the results in this study, and the codes are publicly available via Zenodo at https://zenodo.org/records/18914631.

Acknowledgments

We thank all the data providers and climate modelling groups. We also wish to thank the Center for High Performance Computing and System Simulation, Pilot National Laboratory for Marine Science and Technology (Qingdao) for providing computing resource.

Funding Statements

J.L. acknowledges the support from the National Natural Science Foundation of China (NSFC) Project (42288101), Laoshan Laboratory (No. LSKJ202202600) and Shandong Natural Science Foundation Project (ZR2019ZD12). M.C. was supported by NERC NE/S004645/1. H.W. acknowledges the support from China Scholarship Council (No. 202406330057) and Fundamental Research Funds for the Central Universities (202561008). F.Z. and F.L. declare no relevant funding.

Contributions

H.W., J.L. and M.C. designed the research. H.W. performed the analysis and drafted the paper. H.W., J.L., F.Z., M.C. and F.L. discussed the design, methods and results and contributed to the writing of the paper. All authors gave final approval for publication.

Competing interests

The authors declare no competing interests.

References

1. Alexander, L. V *et al.* Global observed changes in daily climate extremes of temperature and precipitation. *Journal of Geophysical Research: Atmospheres* **111**, (2006).
2. Screen, J. A. Arctic amplification decreases temperature variance in northern mid- to high-latitudes. *Nat. Clim. Chang.* **4**, 577–582 (2014).
3. Perkins-Kirkpatrick, S. E. & Lewis, S. C. Increasing trends in regional heatwaves. *Nat. Commun.* **11**, 3357 (2020).
4. Weather and Climate Extreme Events in a Changing Climate. in *Climate Change 2021 – The Physical Science Basis: Working Group I Contribution to the Sixth Assessment Report of the Intergovernmental Panel on Climate Change* (ed. IPCC) 1513–1766 (Cambridge University Press, Cambridge, 2023). doi:DOI: 10.1017/9781009157896.013.
5. Vautard, R. *et al.* Heat extremes in Western Europe increasing faster than simulated due to atmospheric circulation trends. *Nat. Commun.* **14**, 6803 (2023).
6. Simmons, A. J. Trends in the tropospheric general circulation from 1979 to 2022. *Weather Clim. Dynam.* **3**, 777–809 (2022).
7. Fischer, E. M. *et al.* Record-breaking extremes in a warming climate. *Nat. Rev. Earth Environ.* **6**, 456–470 (2025).
8. Mori, M., Kosaka, Y., Watanabe, M., Nakamura, H. & Kimoto, M. A reconciled estimate of the influence of Arctic sea-ice loss on recent Eurasian cooling. *Nat. Clim. Chang.* **9**, 123–129 (2019).
9. Cohen, J. *et al.* Divergent consensuses on Arctic amplification influence on midlatitude severe winter weather. *Nat. Clim. Chang.* **10**, 20–29 (2020).
10. Cohen, J., Agel, L., Barlow, M., Garfinkel, C. I. & White, I. Linking Arctic variability and change with extreme winter weather in the United States. *Science (1979).* **373**, 1116–1121 (2021).

11. Yao, Y. *et al.* Extreme Cold Events in North America and Eurasia in November-December 2022: A Potential Vorticity Gradient Perspective. *Adv. Atmos. Sci.* **40**, 953–962 (2023).
12. Van Oldenborgh, G. J. *et al.* Cold waves are getting milder in the northern midlatitudes. *Environmental Research Letters* **14**, 114004 (2019).
13. Dunn, R. J. H. *et al.* Development of an Updated Global Land In Situ-Based Data Set of Temperature and Precipitation Extremes: HadEX3. *Journal of Geophysical Research: Atmospheres* **125**, e2019JD032263 (2020).
14. Li, C. *et al.* Changes in Annual Extremes of Daily Temperature and Precipitation in CMIP6 Models. *J. Clim.* **34**, 3441–3460 (2021).
15. Blackport, R., Sigmond, M. & Screen, J. A. Models and observations agree on fewer and milder midlatitude cold extremes even over recent decades of rapid Arctic warming. *Sci. Adv.* **10**, eadp1346 (2024).
16. Blackport, R. & Fyfe, J. C. Amplified warming of North American cold extremes linked to human-induced changes in temperature variability. *Nat. Commun.* **15**, 5864 (2024).
17. Fischer, E. M. & Knutti, R. Heated debate on cold weather. *Nat. Clim. Chang.* **4**, 537–538 (2014).
18. Sippel, S. *et al.* Could an extremely cold central European winter such as 1963 happen again despite climate change? *Weather and Climate Dynamics* **5**, 943–957 (2024).
19. Overland, J. E., Wood, K. R. & Wang, M. Warm Arctic—cold continents: climate impacts of the newly open Arctic Sea. *Polar Res.* **30**, 15787 (2011).
20. Cohen, J. L., Furtado, J. C., Barlow, M. A., Alexeev, V. A. & Cherry, J. E. Arctic warming, increasing snow cover and widespread boreal winter cooling. *Environmental Research Letters* **7**, 014007 (2012).
21. Cohen, J., Pfeiffer, K. & Francis, J. A. Warm Arctic episodes linked with increased frequency of extreme winter weather in the United States. *Nat. Commun.* **9**, 869 (2018).
22. Cohen, J., Agel, L., Barlow, M. & Entekhabi, D. No detectable trend in mid-latitude cold extremes during the recent period of Arctic amplification. *Commun. Earth Environ.* **4**, 341 (2023).
23. Johnson, N. C., Xie, S.-P., Kosaka, Y. & Li, X. Increasing occurrence of cold and warm extremes during the recent global warming slowdown. *Nat. Commun.* **9**, 1724 (2018).
24. Ye, K. & Messori, G. Two Leading Modes of Wintertime Atmospheric Circulation Drive the Recent Warm Arctic–Cold Eurasia Temperature Pattern. *J. Clim.* **33**, 5565–5587 (2020).
25. Francis, J. A. & Vavrus, S. J. Evidence linking Arctic amplification to extreme weather in mid-latitudes. *Geophys. Res. Lett.* **39**, (2012).
26. Francis, J. A. & Vavrus, S. J. Evidence for a wavier jet stream in response to rapid Arctic warming. *Environmental Research Letters* **10**, 014005 (2015).
27. Vavrus, S. J. The Influence of Arctic Amplification on Mid-latitude Weather and Climate. *Curr. Clim. Change Rep.* **4**, 238–249 (2018).
28. Schneider, T., Bischoff, T. & Płotka, H. Physics of Changes in Synoptic Midlatitude Temperature Variability. *J. Clim.* **28**, 2312–2331 (2015).
29. Dai, A. & Deng, J. Arctic Amplification Weakens the Variability of Daily Temperatures over Northern Middle-High Latitudes. *J. Clim.* **34**, 2591–2609 (2021).
30. Peterson, T. C., Zhang, X., Brunet-India, M. & Vázquez-Aguirre, J. L. Changes in North American extremes derived from daily weather data. *Journal of Geophysical Research: Atmospheres* **113**, (2008).

31. Blackport, R. & Screen, J. A. Weakened evidence for mid-latitude impacts of Arctic warming. *Nat. Clim. Chang.* **10**, 1065–1066 (2020).
32. Blackport, R., Fyfe, J. C. & Screen, J. A. Decreasing subseasonal temperature variability in the northern extratropics attributed to human influence. *Nat. Geosci.* **14**, 719–723 (2021).
33. Walsh, J. E., Phillips, A. S., Portis, D. H. & Chapman, W. L. Extreme Cold Outbreaks in the United States and Europe, 1948–99. *J. Clim.* **14**, 2642–2658 (2001).
34. Vavrus, S., Walsh, J. E., Chapman, W. L. & Portis, D. The behavior of extreme cold air outbreaks under greenhouse warming. *International Journal of Climatology* **26**, 1133–1147 (2006).
35. Park, T.-W. *et al.* Different characteristics of cold day and cold surge frequency over East Asia in a global warming situation. *Journal of Geophysical Research: Atmospheres* **116**, (2011).
36. Guo, Y. *et al.* Temperature Variability and Mortality: A Multi-Country Study. *Environ. Health Perspect.* **124**, (2016).
37. Busby, J. W. *et al.* Cascading risks: Understanding the 2021 winter blackout in Texas. *Energy Res. Soc. Sci.* **77**, 102106 (2021).
38. Dai, Y.-L. *et al.* Intensified extreme cold surges in northern East Asia and the associated changes in atmospheric circulation under climate change. *Advances in Climate Change Research* **16**, 960–973 (2025).
39. Ma, L., Wei, Z., Li, X. & Wu, S. Future Changes in Various Cold Surges over China in CMIP6 Projections. *Adv. Atmos. Sci.* **41**, 1751–1768 (2024).
40. Nie, Y., Sun, Y., Zhang, X. & Chen, G. Human-induced changes in extreme cold surges across the Northern Hemisphere. *Nat. Commun.* **16**, 8086 (2025).
41. Song, S. & Yan, X. Projected changes and uncertainty in cold surges over northern China using the CMIP6 weighted multi-model ensemble. *Atmos. Res.* **278**, 106334 (2022).
42. Ding, T., Gao, H. & Li, X. Increasing occurrence of extreme cold surges in North China during the recent global warming slowdown and the possible linkage to the extreme pressure rises over Siberia. *Atmos. Res.* **248**, 105198 (2021).
43. Analitis, A. *et al.* Effects of Cold Weather on Mortality: Results From 15 European Cities Within the PHEWE Project. *Am. J. Epidemiol.* **168**, 1397–1408 (2008).
44. Zhan, Z. *et al.* Temperature change between neighboring days and mortality in United States: A nationwide study. *Science of The Total Environment* **584–585**, 1152–1161 (2017).
45. Sun, Q. *et al.* Health risks and economic losses from cold spells in China. *Science of The Total Environment* **821**, 153478 (2022).
46. D'Amato, M. *et al.* The impact of cold on the respiratory tract and its consequences to respiratory health. *Clin. Transl. Allergy* **8**, 20 (2018).
47. Hyrkäs-Palmu, H. *et al.* Cold weather increases respiratory symptoms and functional disability especially among patients with asthma and allergic rhinitis. *Sci. Rep.* **8**, 10131 (2018).
48. Lo, Y. T. E., Mitchell, D. M. & Gasparrini, A. Compound mortality impacts from extreme temperatures and the COVID-19 pandemic. *Nat. Commun.* **15**, 4289 (2024).
49. Kysely, J., Pokorna, L., Kyncl, J. & Kriz, B. Excess cardiovascular mortality associated with cold spells in the Czech Republic. *BMC Public Health* **9**, 19 (2009).
50. Yang, T.-C., Wu, P.-C., Chen, V. Y.-J. & Su, H.-J. Cold surge: A sudden and spatially varying threat to

health? *Science of The Total Environment* **407**, 3421–3424 (2009).
51. Son, J.-Y., Lee, J.-T., Anderson, G. B. & Bell, M. L. Vulnerability to temperature-related mortality in Seoul, Korea. *Environmental Research Letters* **6**, 034027 (2011).
52. Stewart, S., Keates, A. K., Redfern, A. & McMurray, J. J. V. Seasonal variations in cardiovascular disease. *Nat. Rev. Cardiol.* **14**, 654–664 (2017).
53. Keatinge, W. R. *et al.* Increases in platelet and red cell counts, blood viscosity, and arterial pressure during mild surface cooling: factors in mortality from coronary and cerebral thrombosis in winter. *Br. Med. J. (Clin Res. Ed).* **289**, 1405 (1984).
54. Gasparrini, A. *et al.* Mortality risk attributable to high and low ambient temperature: a multicountry observational study. *The Lancet* **386**, 369–375 (2015).
55. Gasparrini, A. *et al.* Projections of temperature-related excess mortality under climate change scenarios. *Lancet Planet. Health* **1**, e360–e367 (2017).
56. Romanello, M. *et al.* The 2024 report of the Lancet Countdown on health and climate change: facing record-breaking threats from delayed action. *The Lancet* **404**, 1847–1896 (2024).
57. Zhao, W. *et al.* Reliance on fossil fuels increases during extreme temperature events in the continental United States. *Commun. Earth Environ.* **4**, 473 (2023).
58. Bertrand, J.-L. & Parnaudeau, M. Ranking the Impact of Climate Variability on UK Retail Sectors: A Path to Resilience. *SSRN Electronic Journal* https://doi.org/10.2139/ssrn.2675965 (2015) doi:10.2139/ssrn.2675965.
59. Makridis, C. Can You Feel the Heat? Extreme Temperatures, Stock Returns, and Economic Sentiment. *SSRN Electronic Journal* https://doi.org/10.2139/ssrn.3095422 (2018) doi:10.2139/ssrn.3095422.
60. Kotz, M., Wenz, L., Stechemesser, A., Kalkuhl, M. & Levermann, A. Day-to-day temperature variability reduces economic growth. *Nat. Clim. Chang.* **11**, 319–325 (2021).
61. Kotz, M., Levermann, A. & Wenz, L. The economic commitment of climate change. *Nature* **628**, 551–557 (2024).
62. Mohaddes, K., Ng, R. N. C., Pesaran, M. H., Raissi, M. & Yang, J.-C. Climate change and economic activity: evidence from US states. *Oxford Open Economics* **2**, odac010 (2023).
63. Wu, L., Liu, D. & Lin, T. The Impact of Climate Change on Financial Stability. *Sustainability* **15**, 11744 (2023).
64. Zhou, M., Wang, H., Yang, S. & Fan, K. Influence of springtime North Atlantic Oscillation on crops yields in Northeast China. *Clim. Dyn.* **41**, 3317–3324 (2013).
65. Christidis, N. & Stott, P. A. Changes in the geopotential height at 500 hPa under the influence of external climatic forcings. *Geophys. Res. Lett.* **42**, 10, 710–798, 806 (2015).
66. He, C. *et al.* Rising geopotential height under global warming. *Clim. Dyn.* **62**, 5769–5786 (2024).
67. Liu, Z. *et al.* Anthropogenic intensification of Arctic anticyclonic circulation. *Sci. Adv.* **11**, eads4508 (2025).
68. Cohen, J., Francis, J. A. & Pfeiffer, K. Anomalous Arctic warming linked with severe winter weather in Northern Hemisphere continents. *Commun. Earth Environ.* **5**, 557 (2024).
69. Li, J. *et al.* Influence of the NAO on Wintertime Surface Air Temperature over East Asia: Multidecadal Variability and Decadal Prediction. *Adv. Atmos. Sci.* **39**, 625–642 (2022).
70. Wang, H., Li, J., Zheng, F. & Li, F. The synergistic effect of the summer NAO and northwest pacific SST

on extreme heat events in the central–eastern China. *Clim. Dyn.* **61**, 4283–4300 (2023).

71. Wang, H. *et al.* The synergistic effect of the preceding winter mid-latitude North Atlantic and summer tropical eastern Indian Ocean SST on summer extreme heat events in northern China. *Weather Clim. Extrem.* **44**, 100660 (2024).
72. Watanabe, M. *et al.* Possible shift in controls of the tropical Pacific surface warming pattern. *Nature* **630**, 315–324 (2024).
73. Sun, Y. *et al.* Key local atmospheric processes of the heat extreme over the middle-lower Yangtze River basin in August 2022. *Clim. Dyn.* **63**, 268 (2025).
74. Geen, R. *et al.* An Explanation for the Metric Dependence of the Midlatitude Jet-Waviness Change in Response to Polar Warming. *Geophys. Res. Lett.* **50**, e2023GL105132 (2023).
75. Gillett, N. P. *et al.* The Detection and Attribution Model Intercomparison Project (DAMIP v1.0) contribution to CMIP6. *Geosci. Model Dev.* **9**, 3685–3697 (2016).
76. Eyring, V. *et al.* Overview of the Coupled Model Intercomparison Project Phase 6 (CMIP6) experimental design and organization. *Geosci. Model Dev.* **9**, 1937–1958 (2016).
77. Wills, R. C. J., Dong, Y., Proistosecu, C., Armour, K. C. & Battisti, D. S. Systematic Climate Model Biases in the Large-Scale Patterns of Recent Sea-Surface Temperature and Sea-Level Pressure Change. *Geophys. Res. Lett.* **49**, e2022GL100011 (2022).
78. Mori, M., Watanabe, M., Shiogama, H., Inoue, J. & Kimoto, M. Robust Arctic sea-ice influence on the frequent Eurasian cold winters in past decades. *Nat. Geosci.* **7**, 869–873 (2014).
79. Collins, M. *et al.* Emerging signals of climate change from the equator to the poles: new insights into a warming world. *Frontiers in Science* **Volume 2-2024**, (2024).
80. Hersbach, H. *et al.* The ERA5 global reanalysis. *Quarterly Journal of the Royal Meteorological Society* **146**, 1999–2049 (2020).
81. Rayner, N. A. & Others. Global analyses of sea surface temperature, sea ice, and night marine air temperature since the late nineteenth century. *J. Geophys. Res.* **108**, 4407 (2003).
82. Sen, P. K. Estimates of the Regression Coefficient Based on Kendall's Tau. *J. Am. Stat. Assoc.* **63**, 1379–1389 (1968).
83. Kosaka, Y. & Xie, S.-P. Recent global-warming hiatus tied to equatorial Pacific surface cooling. *Nature* **501**, 403–407 (2013).
84. Zhao, S., Li, J. & Sun, C. Decadal variability in the occurrence of wintertime haze in central eastern China tied to the Pacific Decadal Oscillation. *Sci. Rep.* **6**, 27424 (2016).
85. Austin, P. C. & Tu, J. V. Bootstrap Methods for Developing Predictive Models. *Am. Stat.* **58**, 131–137 (2004).

Figure Captions

Fig. 1 | The observed hemispheric divergent trends in winter temperature drop days. a Observed spatial patterns of linear trends in winter temperature drop day frequency from 1979–2024. Hatching indicates that the values are significant at the 95% confidence level based on the Mann-Kendall test. The two black boxes represent the regions for CNWE. **b** Probability distribution of bootstrapped CNWE index anomalies in the periods of 1979–2001 (red) and 2002–2024 (blue). The shaded areas indicate values within the 5% lower and 95% upper confidence bounds, and the solid vertical line indicates the averaged CNWE index anomalies in each period. **c**–**d** Area coverages of trends in winter **c** temperature drop day frequency and **d** air temperature in Northern Hemisphere. The solid (hatched) bars indicate the significant (insignificant) trends at the 95% confidence level based on the Mann-Kendall test. The grey bar indicates no trend.

Fig. 2 | Regional spatially disparate trends in winter temperature drop day frequency from 1979 to 2024. a The time series of CNWE index anomaly. **b** Observed first principal patterns of winter temperature drop day frequency. **c** Standardized first principal time series of winter temperature drop day frequency.

Fig. 3 | Observed trends in winter atmospheric circulation from 1979 to 2024 and their zonal asymmetry. a–**b** Observed trends in winter geopotential height at **a** 200 hPa and **b** 500 hPa. Stippling indicates that the values are significant at the 95% confidence level based on the Mann-Kendall test. **c**–**d** The zonal asymmetry component of the observed trends in geopotential height at **c** 200 hPa and **d** 500 hPa. The zonal asymmetry components are calculated by subtracting the zonal mean from the local trend presented in **a** and **b** at each latitude.

Fig. 4 | Observed trends in winter daily atmospheric circulation variabilities from 1979 to 2024. a Spatial distribution of the linear trends in westerly jet frequency in winter. The westerly jet is defined as the number of days in each winter that the daily 200 hPa zonal wind speed exceeds 30 m s^{-1}. The solid black line indicates the climatological axis of the westerly jet. The position is defined as the location of maximum jet frequency between 45°N–60°N during 1979 to 2024. The spatial distribution of trends relative to this axis highlights the meridional displacement of the jet stream. Stippling indicates that the values are significant at the 95% confidence level based on the Mann-Kendall test. **b** Time series of the frequency of 500–1000 hPa atmospheric thickness drop days over central and western North America (blue) and Northern Europe (red).

Fig. 5 | The difference in CNWE patterns between AMIP and historical simulations in CMIP6 models. a The difference in the linear trends of winter temperature drop day frequency between the multi-model ensemble (MME) mean of AMIP and CMIP6 historical simulations during 1979–2013. **b** The linear trends in the CNWE index in AMIP and CMIP6 historical simulations for each individual model and MME during 1979–2013. The black dashed line represents the linear trends in the CNWE index for ERA5 data during 1979–2024.

Fig. 6 | Detection and attribution of the zonal asymmetry in winter atmospheric circulation trends over polar area. a–f Zonally asymmetric components of trends in winter geopotential height at **a–c** 200 hPa and **d–f** 500 hPa of multi-model ensemble (MME) mean from 1979–2019. **a** and **d** represent the greenhouse gas (GHG) forcing. **b** and **e** represent the aerosol (AER) forcing. **c** and **f** represent the natural (NAT) forcing. The zonally asymmetric components are derived by subtracting the zonal mean trend from the total trend. **g–h** Trends in zonal hemispheric asymmetry of winter geopotential height difference at **g** 200 and **h** 500 hPa under different forcings (1979–2019) and AMIP (1979–2013) simulations. The central line indicates the median, the box bounds represent the interquartile range (IQR; 25th–75th percentiles), and the whiskers extend to the furthest data point within 1.5 times the IQR. The MME is shown by the black diamond, and individual model results are represented as colored dots. The zonal hemispheric asymmetry is defined as the geopotential height difference between the two black boxes: the polar region north of North America (60°–80°N, 90°W–180°) and that north of Europe (60°–80°N, 30°–90°E).

Figures

Figure 1

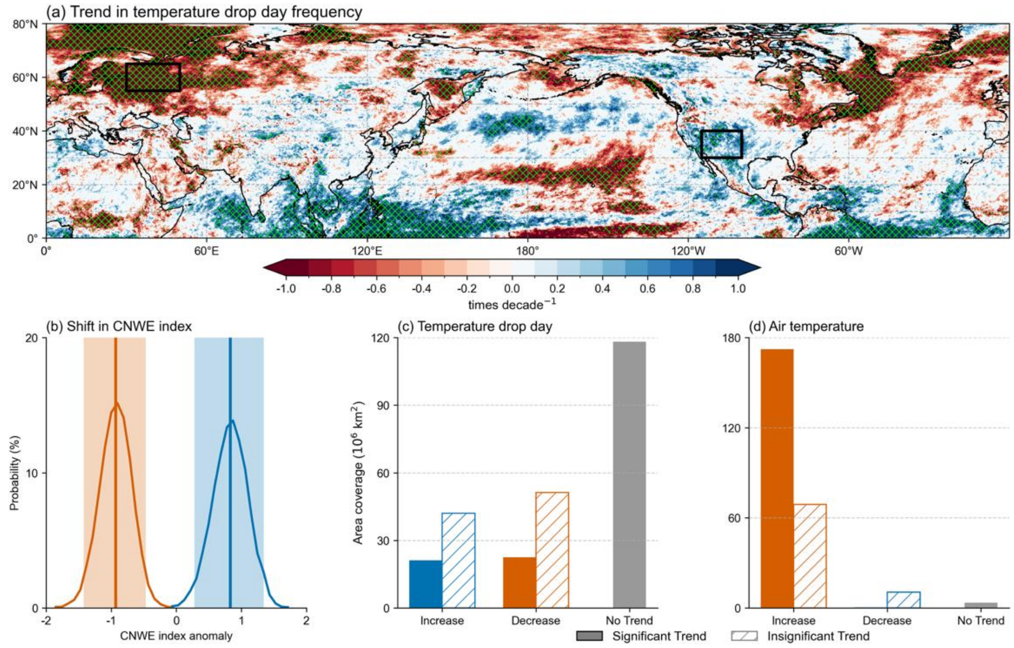

Fig. 1 | The observed hemispheric divergent trends in winter temperature drop days. a Observed spatial patterns of linear trends in winter temperature drop day frequency from 1979–2024. Hatching indicates that the values are significant at the 95% confidence level based on the Mann-Kendall test. The two black boxes represent the regions for CNWE. **b** Probability distribution of bootstrapped CNWE index anomalies in the periods of 1979–2001 (red) and 2002–2024 (blue). The shaded areas indicate values within the 5% lower and 95% upper confidence bounds, and the solid vertical line indicates the averaged CNWE index anomalies in each period. **c**–**d** Area coverages of trends in winter **c** temperature drop day frequency and **d** air temperature in Northern Hemisphere. The solid (hatched) bars indicate the significant (insignificant) trends at the 95% confidence level based on the Mann-Kendall test. The grey bar indicates no trend.

Figure 2

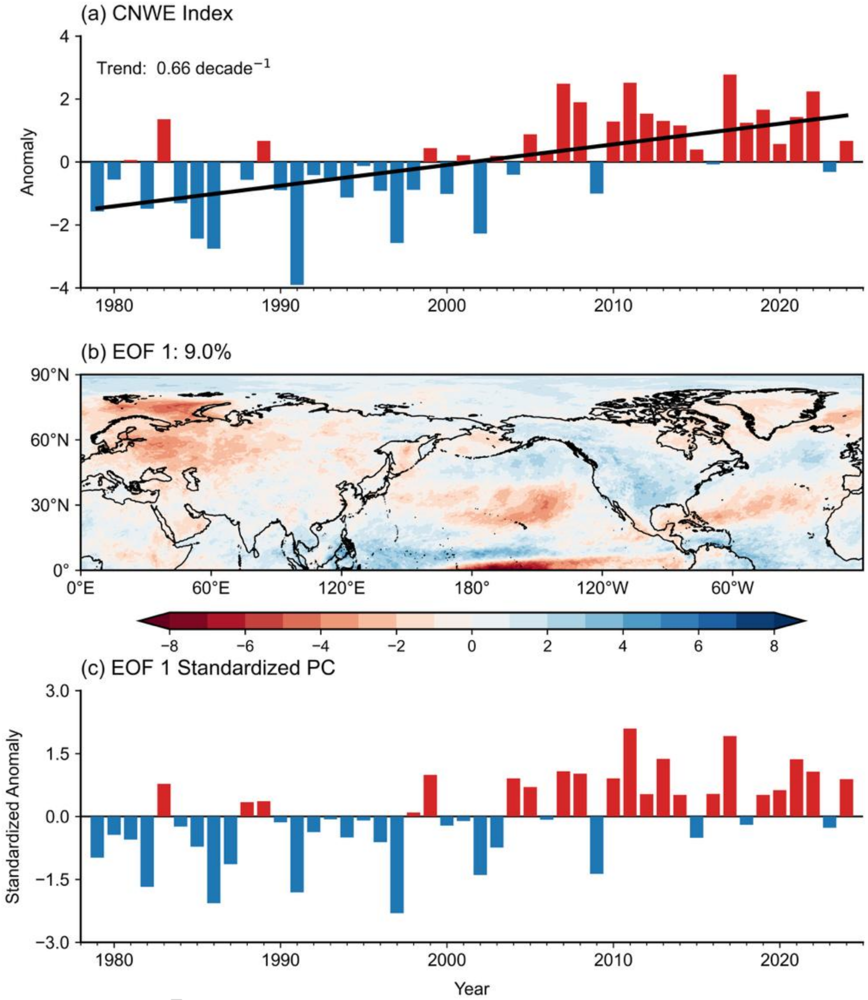

Fig. 2 | Regional spatially disparate trends in winter temperature drop day frequency from 1979 to 2024. a The time series of CNWE index anomaly. **b** Observed first principal patterns of winter temperature drop day frequency. **c** Standardized first principal time series of winter temperature drop day frequency.

Figure 3

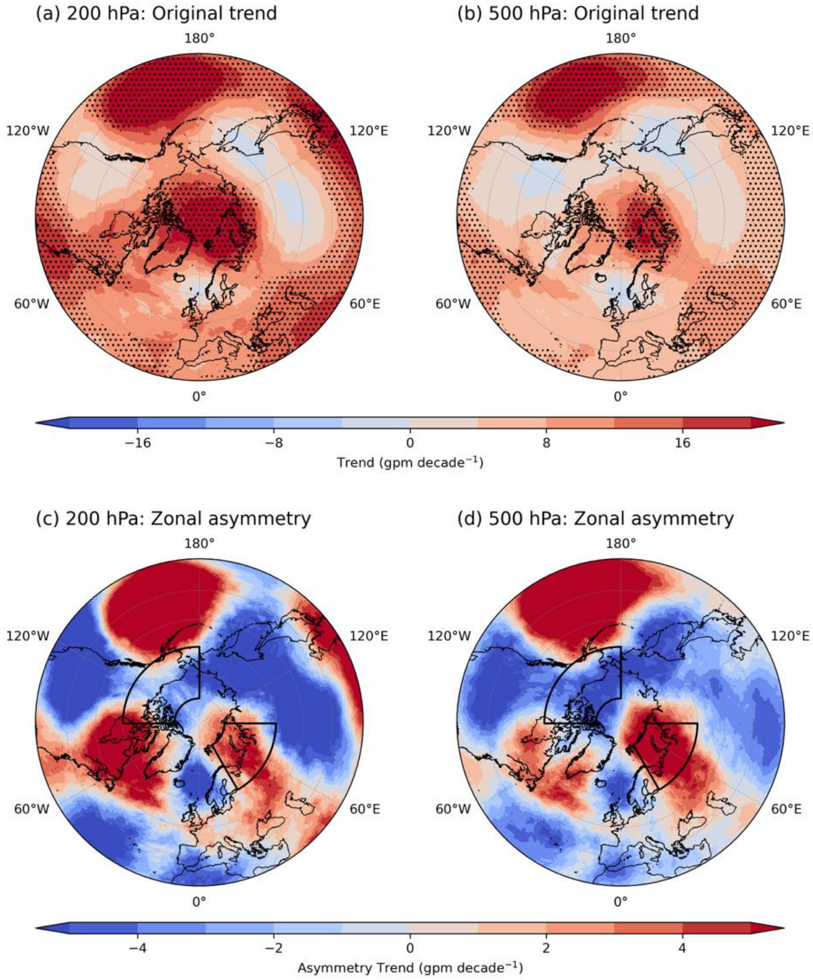

Fig. 3 | Observed trends in winter atmospheric circulation from 1979 to 2024 and their zonal asymmetry. a–**b** Observed trends in winter geopotential height at **a** 200 hPa and **b** 500 hPa. Stippling indicates that the values are significant at the 95% confidence level based on the Mann-Kendall test. **c**–**d** The zonal asymmetry component of the observed trends in geopotential height at **c** 200 hPa and **d** 500 hPa. The zonal asymmetry components are calculated by subtracting the zonal mean from the local trend presented in **a** and **b** at each latitude.

Figure 4

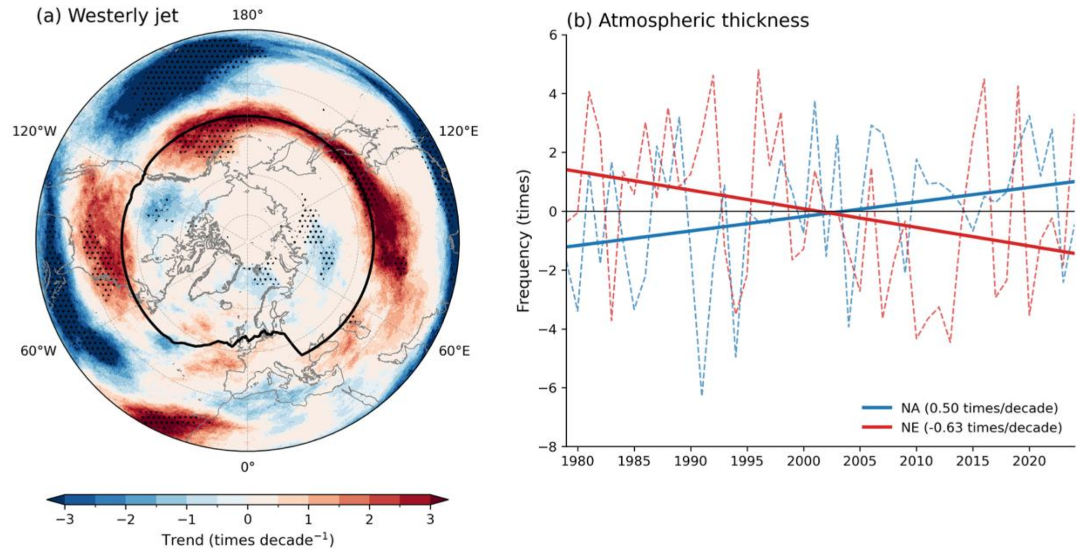

Fig. 4 | Observed trends in winter daily atmospheric circulation variabilities from 1979 to 2024. a Spatial distribution of the linear trends in westerly jet frequency in winter. The westerly jet is defined as the number of days in each winter that the daily 200 hPa zonal wind speed exceeds 30 m s^{-1}. The solid black line indicates the climatological axis of the westerly jet. The position is defined as the location of maximum jet frequency between 45°N–60°N during 1979 to 2024. The spatial distribution of trends relative to this axis highlights the meridional displacement of the jet stream. Stippling indicates that the values are significant at the 95% confidence level based on the Mann-Kendall test. **b** Time series of the frequency of 500–1000 hPa atmospheric thickness drop days over central and western North America (blue) and Northern Europe (red).

Figure 5

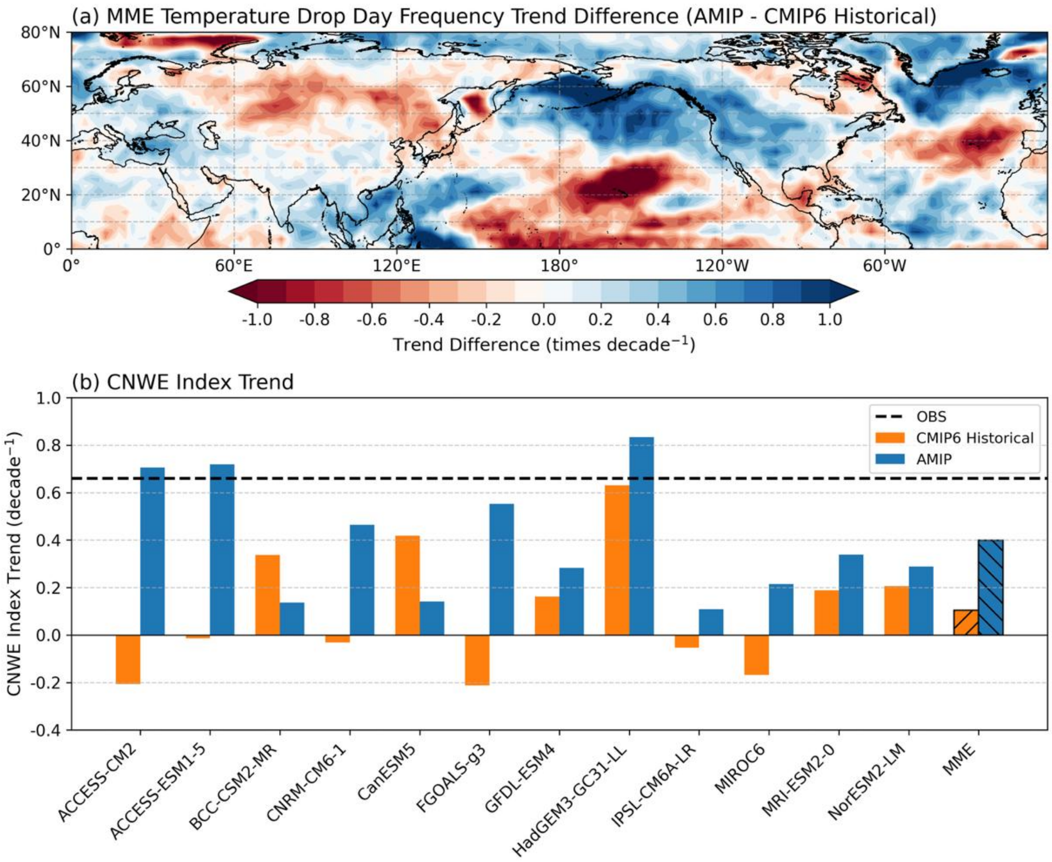

Fig. 5 | The difference in CNWE patterns between AMIP and historical simulations in CMIP6 models. a The difference in the linear trends of winter temperature drop day frequency between the multi-model ensemble (MME) mean of AMIP and CMIP6 historical simulations during 1979–2013. **b** The linear trends in the CNWE index in AMIP and CMIP6 historical simulations for each individual model and MME during 1979–2013. The black dashed line represents the linear trends in the CNWE index for ERA5 data during 1979–2024.

Figure 6

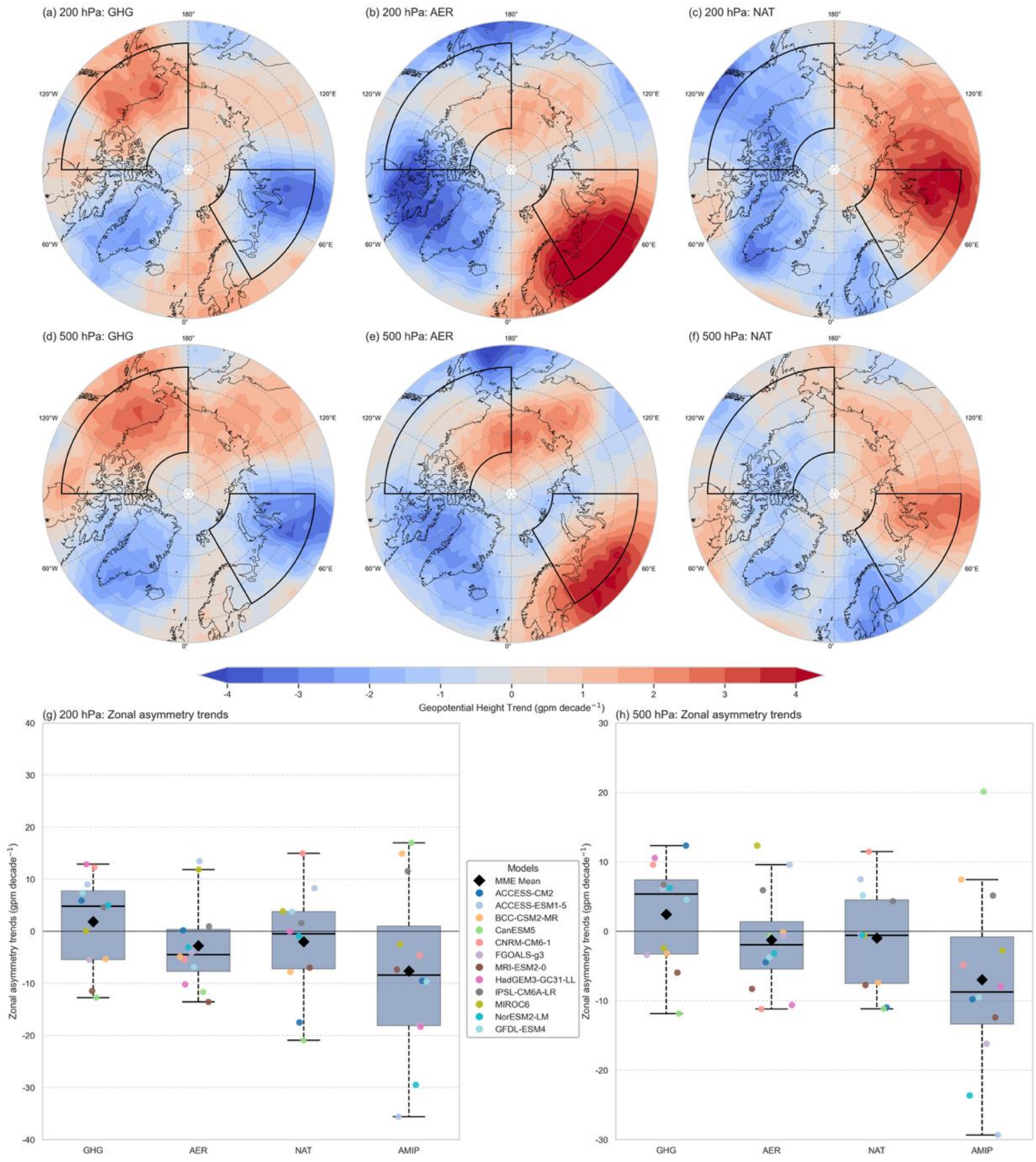

Fig. 6 | Detection and attribution of the zonal asymmetry in winter atmospheric circulation trends over polar area. a–f Zonally asymmetric components of trends in winter geopotential height at **a–c** 200 hPa and **d–f** 500 hPa of multi-model ensemble (MME) mean from 1979–2019. **a** and **d** represent the greenhouse gas (GHG) forcing. **b** and **e** represent the aerosol (AER) forcing. **c** and **f** represent the natural (NAT) forcing. The zonally asymmetric components are derived by subtracting the zonal mean trend from the total trend. **g–h** Trends in zonal hemispheric asymmetry of winter geopotential height difference at **g** 200 and **h** 500 hPa under different forcings (1979–2019) and AMIP (1979–2013) simulations. The central line indicates the median, the box bounds represent the interquartile range (IQR; 25th–75th percentiles), and the whiskers extend to the furthest data point within 1.5 times the IQR. The MME is shown by the black diamond, and individual model results are represented as colored dots. The zonal hemispheric asymmetry is defined as the geopotential height difference between the two black boxes: the polar region north of North America (60°–80°N, 90°W–180°) and that north of Europe (60°–80°N, 30°–90°E).

Editorial summary:

Occurrence of winter temperature drop days increased in North America but declined in Europe over the past four decades due to changes in tropospheric polar vortex, revealed by attribution analyses based on climate models.

Peer review information:

Communications Earth and Environment thanks Judah Cohen and the other, anonymous, reviewer(s) for their contribution to the peer review of this work. Primary Handling Editors: Kyung-Sook Yun and ChenRui Diao. A peer review file is available.